NDRG1 functions in LDL receptor trafficking by regulating endosomal recycling and degradation

Vilja Pietiäinen[1,2,*], Boris Vassilev[1,3], Tomas Blom[1,3], Wei Wang[1,3], Jessica Nelson[4], Robert Bittman[5], Nils Bäck[1], Noam Zelcer[4] and Elina Ikonen[1,3]

[1]Institute of Biomedicine, Anatomy, University of Helsinki, Helsinki, Finland
[2]Institute for Molecular Medicine Finland FIMM, University of Helsinki, Helsinki, Finland
[3]Minerva Foundation Institute for Medical Research, Helsinki, Finland
[4]Department of Medical Biochemistry, Academic Medical Center, University of Amsterdam, Amsterdam, The Netherlands
[5]Department of Chemistry and Biochemistry, Queens College of The City University of New York, Flushing, NY, USA
*Author for correspondence (vilja.pietiainen@helsinki.fi)

Accepted 17 May 2013
Journal of Cell Science 126, 3961–3971

doi: 10.1242/jcs.128132

Summary

N-myc downstream-regulated gene 1 (NDRG1) mutations cause Charcot–Marie–Tooth disease type 4D (CMT4D). However, the cellular function of NDRG1 and how it causes CMT4D are poorly understood. We report that NDRG1 silencing in epithelial cells results in decreased uptake of low-density lipoprotein (LDL) due to reduced LDL receptor (LDLR) abundance at the plasma membrane. This is accompanied by the accumulation of LDLR in enlarged EEA1-positive endosomes that contain numerous intraluminal vesicles and sequester ceramide. Concomitantly, LDLR ubiquitylation is increased but its degradation is reduced and ESCRT (endosomal sorting complex required for transport) proteins are downregulated. Co-depletion of IDOL (inducible degrader of the LDLR), which ubiquitylates the LDLR and promotes its degradation, rescues plasma membrane LDLR levels and LDL uptake. In murine oligodendrocytes, Ndrg1 silencing not only results in reduced LDL uptake but also in downregulation of the oligodendrocyte differentiation factor Olig2. Both phenotypes are rescued by co-silencing of Idol, suggesting that ligand uptake through LDLR family members controls oligodendrocyte differentiation. These findings identify NDRG1 as a novel regulator of multivesicular body formation and endosomal LDLR trafficking. The deficiency of functional NDRG1 in CMT4D might impair lipid processing and differentiation of myelinating cells.

Key words: Endocytosis, Cholesterol, IDOL, Multivesicular body, NDRG1

Introduction

Low-density lipoprotein (LDL)-cholesterol is internalized into cells by clathrin-mediated endosytosis of the LDL receptor (LDLR) to meet cellular cholesterol needs (Goldstein and Brown, 2009; Ikonen, 2008). In endosomes, LDLR disassociates from LDL particles because of the acidic pH and returns to the plasma membrane (PM). Alternatively, recycling of the LDLR to the PM can be prevented by proprotein convertase subtilisin/kexin type 9 (PCSK9) or by the E3 ubiquitin ligase, inducible degrader of the LDLR (IDOL), which promotes ubiquitylation of the LDLR under conditions of excess cellular sterols (Zelcer et al., 2009). The ability of PCSK9 to alter LDLR levels is independent of, and additive with, the IDOL pathway and does not require LDLR ubiquitylation (Wang et al., 2012; Zhang et al., 2012). Ubiquitylation is an established signal for controlling endocytosis and sorting of membrane receptors, such as the LDLR, to multivesicular bodies (MVBs) and further to lysosomes for degradation (Mukhopadhyay and Riezman, 2007; Piper and Katzmann, 2007; Zelcer et al., 2009). From early endosomes, LDL particles are transported to MVBs/late endosomes (Goldstein and Brown, 2009) for the hydrolysis of LDL-cholesterol esters to free cholesterol (FC) by acid lipase (Sugii et al., 2003) and exit of cholesterol from the late endosomes by Niemann–Pick type C1 and 2 (NPC1 and NPC2) proteins (Carstea et al., 1997; Loftus et al., 1997).

Our interest in the possibility that N-myc downstream regulated gene 1 (NDRG1) might be involved in cellular cholesterol metabolism was initiated by Affymetrix gene expression profiling of cholesterol loaded, NPC1-deficient murine macrophages (Hölttä-Vuori et al., 2012). In this experiment, we identified NDRG1 as one of the highly induced genes in response to cholesterol loading (E. I., unpublished observations). Interestingly, a genome-wide expression analysis of NPC disease fibroblasts found that NDRG1 mRNA is also elevated in these patient-derived cells (Reddy et al., 2006). Moreover, in an RNAi screen focused on cellular lipid phenotypes, NDRG1 was identified as a gene potentially affecting cellular cholesterol levels (Bartz et al., 2009). Yet, how NDRG1 affects cholesterol homeostasis remains unknown.

NDRG1 is widely expressed, with particularly high levels in the nervous system (Lachat et al., 2002). It participates in diverse cellular functions, such as differentiation (van Belzen et al., 1997) and proliferation (Piquemal et al., 1999). NDRG1 expression is often altered in neoplasms, where it can act either as a tumor promoter or suppressor (Bandyopadhyay et al., 2003; Guan et al., 2000). In the demyelinating neuropathy Charcot-Marie–Tooth disease 4D (CMT4D), the deficiency of functional NDRG1 leads to autonomous dysfunction of Schwann cells, the glial cells of the peripheral nervous system (PNS) (Kalaydjieva

Journal of Cell Science

et al., 2000; Kalaydjieva et al., 1996). CMT4D can also be accompanied by abnormalities of the central nervous system (CNS) white matter (Echaniz-Laguna et al., 2007) and functional CNS disturbances (Kalaydjieva et al., 1998).

Subcellularly, NDRG1 is mostly found in the cytoplasm (Lachat et al., 2002) and in endosomes (Kachhap et al., 2007). NDRG1 can interact with proteins involved in vesicular trafficking, and was reported to regulate the recycling of E-cadherin by acting as an effector protein for Rab4a (Kachhap et al., 2007). NDRG1 also binds to prenylated Rab acceptor-1 (PRA1; also known as YIP3, RABAC1) (Hunter et al., 2005; Kim et al., 2012; King et al., 2011), which can act as a GDI displacement factor for endosomal Rab proteins, such as Rab4, Rab5, Rab7 and Rab9 (Bucci et al., 1999; Sivars et al., 2003). How these interactions contribute to the physiological function of NDRG1 or to the consequences of NDRG1 deficiency are poorly understood.

In this study, we describe a role for NDRG1 in cellular lipid homeostasis and endocytic trafficking of the LDLR. Our data further implicate NDRG1 as an important regulator of endosomal maturation that is required for efficient uptake of LDL receptor family members in both epithelial and glial cells.

Results

NDRG1 affects cellular cholesterol distribution and content

To assess whether the endosomal cholesterol content affects the abundance of the NDRG1 protein, we treated epithelial A431 cells with the hydrophobic amine U18666A. This compound induces lysosomal cholesterol accumulation, mimicking the loss of NPC1 function (Ko et al., 2001). Treatment of A431 cells with U18666A resulted in an approximately threefold increase in the endogenous NDRG1 protein content, in line with the upregulation of NDRG1 mRNA in NPC fibroblasts (Reddy et al., 2006). Moreover, loading of cells with LDL-cholesterol led to an approximately twofold increase in the NDRG1 protein levels (Fig. 1A). These findings suggest a role for NDRG1 in LDL-cholesterol trafficking.

To study whether NDRG1 affects cellular cholesterol homeostasis, we silenced NDRG1 using small interfering RNAs (siRNA) in A431 cells. NDRG1 knockdown (k/d) was assessed by immunoblotting, showing consistently a ~90% reduction (89±7% s.e.m.) in NDRG1 protein amount (supplementary material Fig. S1A,B). To examine cholesterol distribution in NDRG1 k/d cells, the cells were stained with filipin, a widely used fluorescent sterol-binding polyene antibiotic. NDRG1 silencing resulted in the redistribution of free cholesterol (FC) from the PM to perinuclear, punctate structures (Fig. 1B). Biochemical lipid analysis revealed that NDRG1 silencing was associated with a decreased cellular cholesterol content. Specifically, while FC remained essentially unchanged upon NDRG1 k/d, an approximately fourfold reduction was observed in cholesterol esters (CE; Fig. 1C). No major changes in cholesterol biosynthesis or efflux to apolipoprotein A-I (apoA-I) were observed in NDRG1 k/d cells (the ratio of values in NDRG1-silenced cells to control cells was 1.26±0.11 and 1.22±0.06, respectively). These data indicate that NDRG1 depletion leads to an abnormal endosomal distribution of FC. Furthermore, as cholesterol biosynthesis and efflux were not substantially affected by NDRG1 k/d, the reduction in the CE content could result from decreased cellular cholesterol uptake.

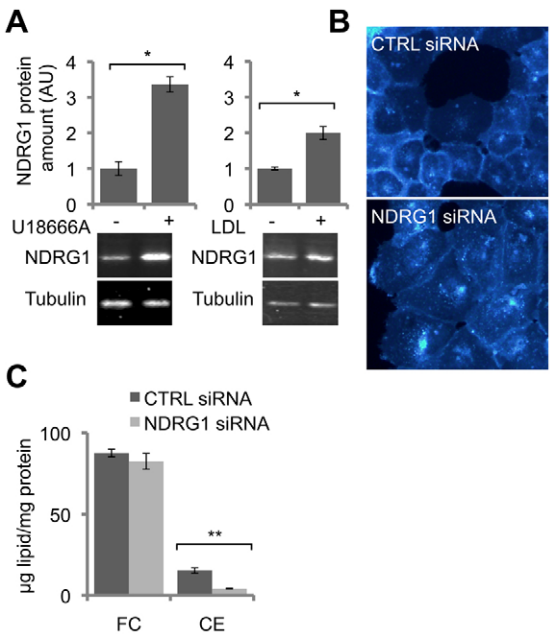

Fig. 1. NDRG1 is regulated by endosomal cholesterol loading and its depletion affects cholesterol distribution and amount. (**A**) U18666A or LDL loading increases cellular NDRG1 protein content. A431 cells were treated with U18666A (1 µg/ml) in 10% FBS for 48 hours or with LDL (50 µg/ml) in serum-free medium for 18 hours, followed by western blotting of NDRG1 and β-tubulin as a loading control. $n=4$–6 samples; values are means ± s.e.m., $^{*}P<0.05$ (Student's t-test). (**B**) Cholesterol distribution is affected by NDRG1 silencing in A431 cells. Cells were transfected with control (CTRL) or NDRG1 siRNAs for 72 hours, fixed, and stained with filipin. (**C**) Cholesterol ester (CE) content is decreased upon NDRG1 k/d. After siRNA treatment of A431 cells, the lipids were extracted and analyzed by TLC. Free cholesterol (FC) and CEs were quantified by densitometry. Results of a representative (means ± s.d.) of three independent experiments with comparable results are shown. $^{**}P<0.001$ (Student's t-test).

Decreased LDLR plasma membrane localization and degradation leads to diminished LDL uptake in NDRG1 -depleted cells

To test whether NDRG1 depletion affects LDL uptake, we monitored the binding and internalization of 1,1′-dioctadecyl-3,3,3′,3′-tetramethyl-indocarbocyanine-perchlorate-labeled LDL (DiI–LDL) in NDRG1 siRNA-transfected A431 cells. LDL uptake was visualized by fluorescence microscopy and quantified by measuring the fluorescence intensity in cell lysates. These assays revealed that both the binding and internalization of DiI–LDL were severely (up to ~50%) diminished upon NDRG1 k/d (Fig. 2A; see also supplementary material Fig. S1C). This phenotype could, in principle, result from decreased LDLR levels. Unexpectedly, the total LDLR protein content was found to be increased upon NDRG1 silencing (Fig. 2B; see also supplementary material Fig. S1B). Biotinylation of the PM pool of LDLR, revealed, however, a clear decrease in the fraction of LDLR in the PM of NDRG1 k/d cells (Fig. 2B). To follow the intracellular degradation of PM LDLR, the biotinylated receptors were internalized for 0–5 hours, pulled down by streptavidin beads, and detected with an anti-LDLR antibody by immunoblotting. In control-siRNA-treated cells, ~80% of the biotinylated LDLR was degraded in 5 hours. However, in NDRG1 k/d cells, degradation of the LDLR

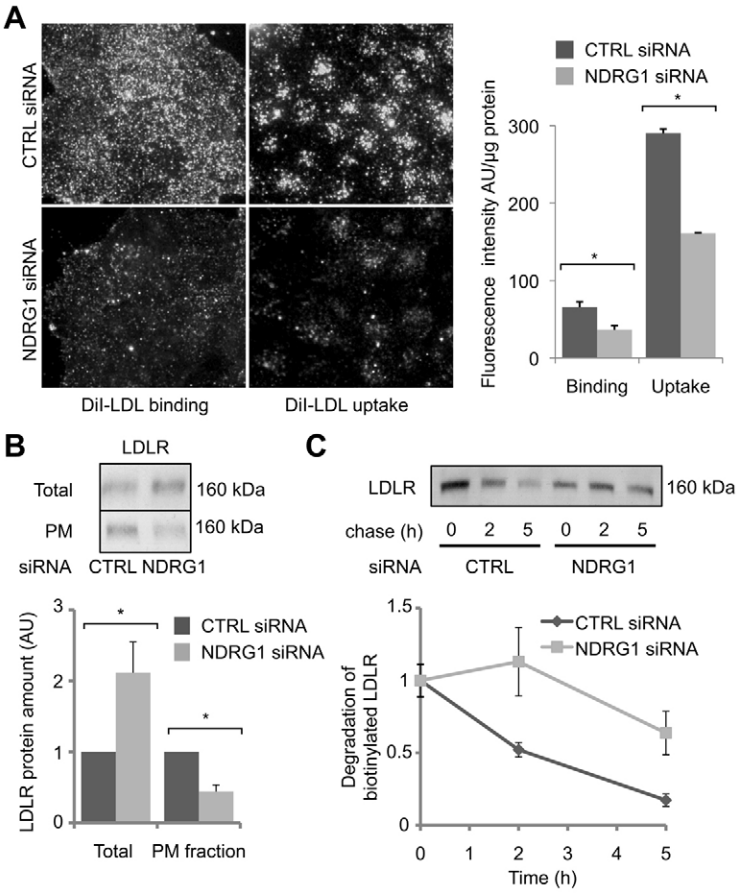

Fig. 2. NDRG1 depletion results in diminished LDL uptake, and decreased PM localization and degradation of LDLR. (**A**) NDRG1 depletion decreases the binding and uptake of DiI–LDL. siRNA-transfected A431 cells were incubated with 5 µg/ml DiI–LDL for 30 minutes at 4℃ (binding) or 20 minutes at 37℃ (uptake), and imaged with a wide-field microscope immediately post-fixation. Cellular fluorescence intensity was quantified from cell lysates, and normalized to the protein amounts (right panel). Values are means ± s.e.m, *$P<0.05$ (Student's *t*-test). (**B**) Total LDLR is increased but the PM fraction of LDLR is decreased in NDRG1 k/d cells. siRNA-transfected A431 cells were subjected to cell-surface biotinylation and streptavidin pull-down. LDLR amounts were analyzed by western blotting and quantified by densitometry; Total, input protein; PM, pull-down of biotinylated PM protein. Values are means ± s.e.m. of three to five experiments, *$P<0.05$ (Student's *t*-test). (**C**) LDLR degradation is slowed down in NDRG1-silenced cells. After surface biotinylation, cells were incubated for the indicated times at 37℃ to allow internalization and degradation of biotinylated LDLR, before analysis as in B. Please note that PM LDLR levels at 0 hours were set as 1; in CTRL-siRNA-treated samples there was an approximate twofold more LDLR at the PM than in NDRG1-siRNA-treated samples. Values are means ± s.e.m. of three samples/condition from two independent experiments.

was severely attenuated with less than 40% of the receptor lost in 5 hours (Fig. 2C). Together, these results demonstrate that NDRG1 is required for the proper PM localization of the LDLR. The reduction of LDLR at the PM results in diminished LDL-cholesterol uptake and is accompanied by retarded degradation of the LDLR.

Silencing of NDRG1 or its interaction partner PRA1 leads to endosomal LDLR sequestration

To define the intracellular localization of excess LDLRs in NDRG1-silenced cells, LDLR was co-immunostained with markers for early endosomes (endosomal antigen 1; EEA1) and late endosomes/lysosomes (Lysosome-associated membrane glycoprotein 1; LAMP1) and imaged by confocal microscopy. In control cells, LDLR typically localized to small, punctate EEA1-positive endosomes in the perinuclear region and to some extent to LAMP1-positive late endosomes/lysosomes (Fig. 3A). In NDRG1-silenced cells, enlarged endosomes and lysosomes were more irregularly scattered in the cytoplasm. Strikingly, the LDLR was largely sequestered in the abnormal EEA1-positive endosomal vesicles (Fig. 3A). These structures also accumulated FC, as detected by filipin staining (supplementary material Fig. S2).

To investigate how NDRG1 deficiency results in the strikingly altered endosome morphology, we considered the involvement of the previously described NDRG1 interaction partners Rab4a and PRA1 (Hunter et al., 2005; Kachhap et al., 2007; Kim et al., 2012; King et al., 2011). Therefore, we tested the consequences of Rab4a or PRA1 silencing on LDLR distribution by immunostaining of A431 cells. We observed that the LDLR phenotype of Rab4a depletion was not identical to that of NDRG1 depletion, with the latter leading to larger intracellular LDLR-positive accumulations (Fig. 3B). However, depletion of PRA1 led to the appearance of enlarged early endosomes and late endosomes (Fig. 3C) as well as to the accumulation of the LDLR in these enlarged EEA1-positive endosomes, closely resembling the LDLR phenotype of NDRG1 k/d cells. We then analyzed whether NDRG1 silencing affects the levels of endogenous PRA1 or endosomal Rab proteins in A431 cells. Remarkably, we observed a significant decrease in the amount of endogenous PRA1 protein, both by immunostaining and immunoblotting of NDRG1 k/d cells (Fig. 4A; see also supplementary material Fig. S3). In contrast, the levels of Rab4, 5 and 7 were not substantially altered (supplementary material Fig. S4).

To address whether the reduced levels of PRA1 contribute to the LDLR trafficking defect observed upon NDRG1 depletion, we overexpressed PRA1 in NDRG1-depleted cells. After fixation, the cells were immunostained for PRA1 and LDLR and assessed for the degree of LDLR endosomal sequestration. pEGFP was expressed as a control to evaluate the possible effect of transfection on LDLR localization. In control cells overexpressing GFP, LDLR showed a punctate staining throughout the cytoplasm, whereas in NDRG1 k/d cells overexpressing GFP, LDLR was abnormally sequestered as expected (Fig. 4B). Importantly, overexpression of PRA1 partially rescued the LDLR phenotype in NDRG1-siRNA-treated

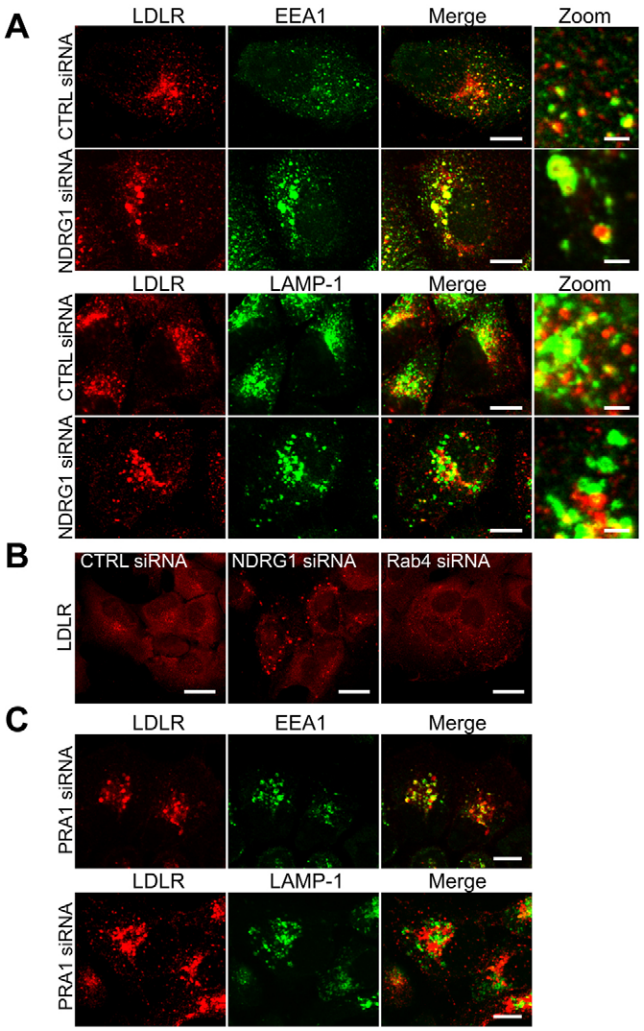

Fig. 3. LDLR accumulates in modified enlarged endosomes upon knockdown of NDRG1 or PRA1. (**A**) LDLR localizes in enlarged endosomes in NDRG1-depleted cells. Confocal images of siRNA-transfected A431 cells, immunostained for LDLR (red), EEA1 (green) and LAMP-1 (green). Scale bars:10 µm (Merge), 5 µm (Zoom). (**B**) Silencing of Rab4a interferes with LDLR distribution in A431 cells but the phenotype differs from that of NDRG1 silencing. Cells were permeabilized with filipin and immunostained with LDLR antibody. Scale bars: 20 µm. (**C**) PRA1 silencing leads to accumulation of LDLR in enlarged EEA1-positive endosomes. Confocal images of PRA1 siRNA-transfected A431 cells, immunostained for LDLR (red) and EEA1 (green) or LAMP1 (green). Scale bars: 10 µm.

cells (Fig. 4B). These results demonstrate that NDRG1 deficiency leads to an abnormal endosomal sequestration of the LDLR. They also suggest that the reduced levels of PRA1 accompanying NDRG1 deficiency might contribute to the aberrant endosomal morphology and LDLR sequestration.

NDRG1 affects the morphology and function of multivesicular bodies

The effect of NDRG1 silencing on the ultrastructure of endosomal organelles was studied by electron microscopy (EM). To this end, siRNA-transfected A431 cells were allowed to internalize BSA-gold for 40 min to label the endosomes and subsequently processed for EM. Both in the control- and NDRG1-silenced cells, BSA-gold accumulated in vesicles with MVB-like morphology (Fig. 5A). For quantification, we measured the diameter of 60 MVBs from unlabeled siRNA-treated EM samples and counted the number of intraluminal vesicles in each. Compared with control cells, MVBs in NDRG1-silenced cells were enlarged and contained approximately threefold more intraluminal vesicles (Fig. 5A).

Because the formation of intraluminal vesicles destined for lysosomal degradation requires endosomal sorting complex required for transport (ESCRT) proteins (Raiborg and Stenmark, 2009), we assessed the levels of the ESCRT components in NDRG1-silenced cells by western blotting. The immunoblots revealed a significant reduction in the amounts of the tested ESCRT proteins, i.e. Hrs (ESCRT-0), TSG101 (ESCRT-I), Vps22 (ESCRT-II), Vps24 (ESCRT-III) and Vps32 (ESCRT-III) (Fig. 5B). In addition to ESCRTs, lipids might play an important role in the membrane invagination step of MVB formation. MVBs are abundant in sphingolipids, such as sphingomyelin (SM) and ceramide, and the latter can induce the formation of internal vesicles in liposomes and trigger budding of exosome vesicles into multivesicular endosomes in cells (Trajkovic et al., 2008). Interestingly, we found a significant increase in the total ceramide levels of NDRG1 k/d cells (Fig. 5C).

To test whether the increase in ceramide is due to its accumulation in the enlarged MVBs, we incorporated a fluorescent derivative of ceramide (BODIPY-labeled ceramide) into LDL particles, and applied them to NDRG1-silenced cells. The cells had been prelabeled overnight with the fluorescent fluid-phase tracer dextran to visualize lysosomes. (Please note that dextran distribution is altered upon NDRG1 depletion due to the redistribution of late endocytic organelles; see supplementary material Fig. S5.) As shown in Fig. 6A, after 1 hour of LDL labeling BODIPY-labeled ceramide was already partially colocalized with dextran in control cells. The extent of colocalization increased until a 2-hour chase, after which it decreased (Fig. 6A). However, in NDRG1 k/d cells, BODIPY-labeled ceramide localized to a lesser extent with dextran after 1 hour of labeling and remained for a prolonged time in enlarged dextran negative vesicular structures (Fig. 6A). This suggests that the transport of ceramide through the endosomal pathway is slower in NDRG1-depleted cells. To address the source of increased endosomal ceramide, we internalized LDL particles labeled with [^{3}H]SM into cells. This revealed increased levels of [^{3}H]SM-derived [^{3}H]ceramide in NDRG1-silenced cells, providing evidence that at least part of the ceramide derives from endosomal SM hydrolysis (Fig. 6B). Together, these findings imply that NDRG1 function is required for proper endosomal maturation. In NDRG1 deficiency, MVBs accumulate increased numbers of intraluminal vesicles despite a marked reduction of ESCRT components. Furthermore, the endosomal retention of both fluorescent ceramide and increased LDL/[^{3}H]SM-derived [^{3}H]ceramide suggests that the intraluminal vesicles in NDRG1-depleted cells are ceramide enriched.

Prevention of IDOL-induced LDLR ubiquitylation rescues LDLR distribution and cholesterol levels in NDRG1-silenced cells

Ubiquitylation of membrane proteins can negatively regulate their cell surface expression by targeting them to the MVBs and for degradation (Staub and Rotin, 2006). Interestingly, silencing

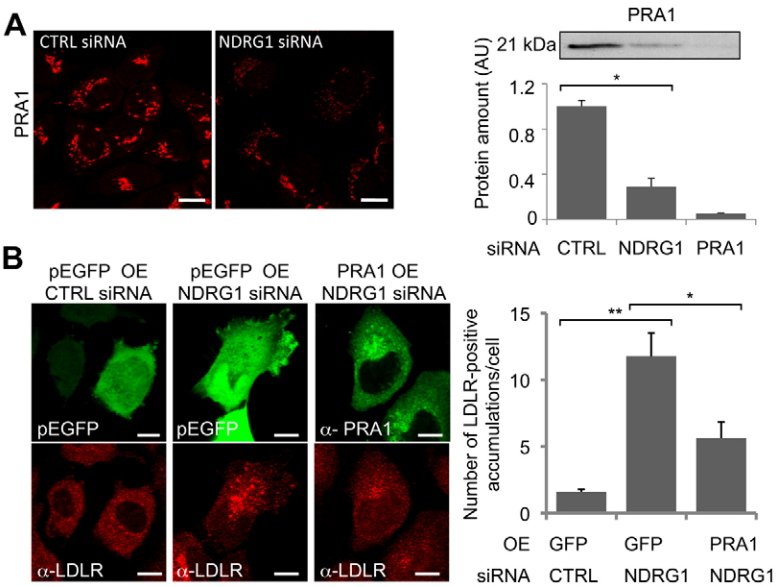

Fig. 4. PRA1 is reduced in NDRG1-silenced cells and its overexpression rescues LDLR distribution in these cells. (**A**) NDRG1 silencing is accompanied by reduced amounts of PRA1. Immunostaining (confocal images) and western blotting of endogenous PRA1 in siRNA-transfected A431 cells. Values are means ± s.e.m. of two to three experiments with parallel samples; *$P<0.05$ (Student's *t*-test). Scale bars: 20 µm. (**B**) PRA1 overexpression (OE) rescues the LDLR accumulation phenotype of NDRG1-silenced cells. PRA1 was overexpressed in NDRG1-silenced A431 cells. Cells overexpressing PRA1 were detected with anti-PRA1 antibody (green), and endogenous LDLR was detected with anti-LDLR antibody (red). pEGFP was used as a transfection control. The number of intracellular LDLR-positive accumulations was quantified from confocal images, $n=70$ cells/sample; values are means ± s.e.m., *$P<0.05$; **$P<0.001$ (Student's *t*-test). Scale bars: 10 µm.

of NDRG1 enhanced the colocalization of the LDLR with ubiquitin in enlarged endosomes (Fig. 7A). This suggests that the abnormal endosomes in NDRG1-silenced cells can accumulate ubiquitin and possibly also ubiquitylated LDLR despite reduced ESCRT levels. To directly analyze whether NDRG1 silencing affects the ubiquitylation status of the LDLR, we used HEK293T cells. The cells were co-transfected with control or NDRG1 siRNAs and an expression plasmid encoding HA-tagged LDLR. The cell lysates were immunoprecipitated with anti-HA beads, followed by immunoblotting with an anti-ubiquitin antibody to detect the ubiquitylated LDLR. As shown in Fig. 7B, depletion of NDRG1 results in increased amounts of ubiquitylated LDLR.

Recently, the E3 ubiquitin ligase IDOL was identified as a novel post-translational regulator of LDLR ubiquitylation (Hong et al., 2010; Sorrentino and Zelcer, 2012; Zelcer et al., 2009). We examined whether prevention of LDLR ubiquitylation by IDOL

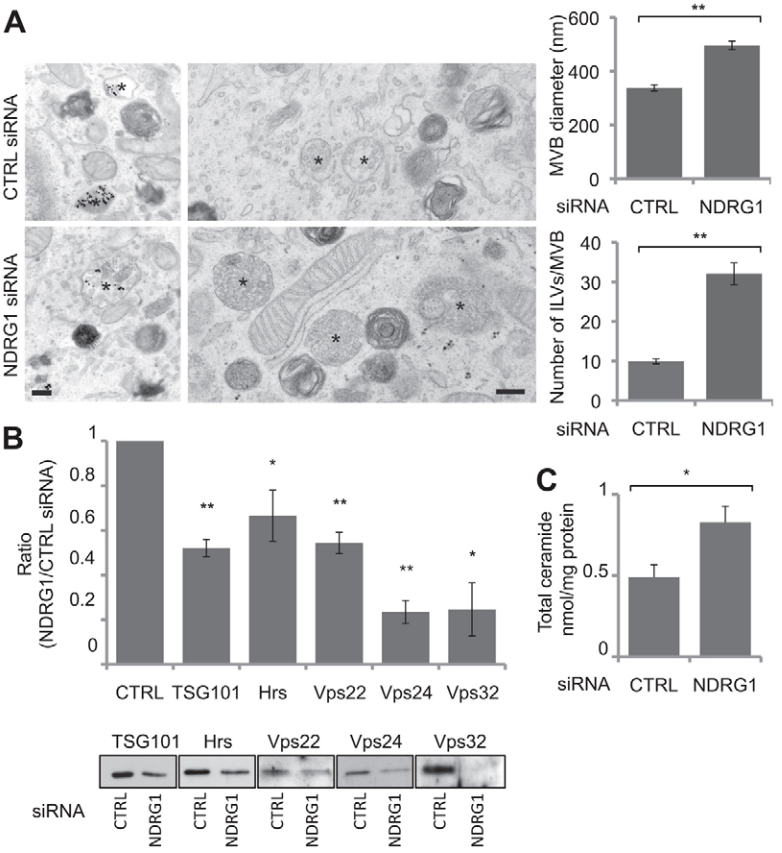

Fig. 5. NDRG1 affects MVB morphology and ESCRT levels. (**A**) NDRG1 silencing results in enlarged MVBs with increased number of intraluminal vesicles. Left: EM images of siRNA-transfected A431 cells, labeled with BSA-gold for 40 minutes. MVBs with ILVs are marked by an asterisk. MVB diameter and the number of intraluminal vesicles (ILVs) were quantified from 60 MVBs of unlabeled EM samples. Values are means ± s.e.m., **$P<0.001$ (Student's *t*-test). Scale bars: 200 nm. (**B**) NDRG1 silencing results in the downregulation of ESCRTs. ESCRT protein amounts relative to CTRL were analyzed by western blotting of siRNA-transfected A431 cells. The representative immunoblots are shown for each ESCRT protein. Values are means ± s.e.m. from two to five independent experiments, *$P<0.05$, **$P<0.001$ (Student's *t*-test). (**C**) Total ceramide content is increased upon NDRG1 depletion in A431 cells. Total cellular ceramide amounts were determined in siRNA-treated A431 cells by HPTLC and densitometry. Values are means ± s.e.m. of five samples/condition from two independent experiments, *$P<0.05$ (Student's *t*-test).

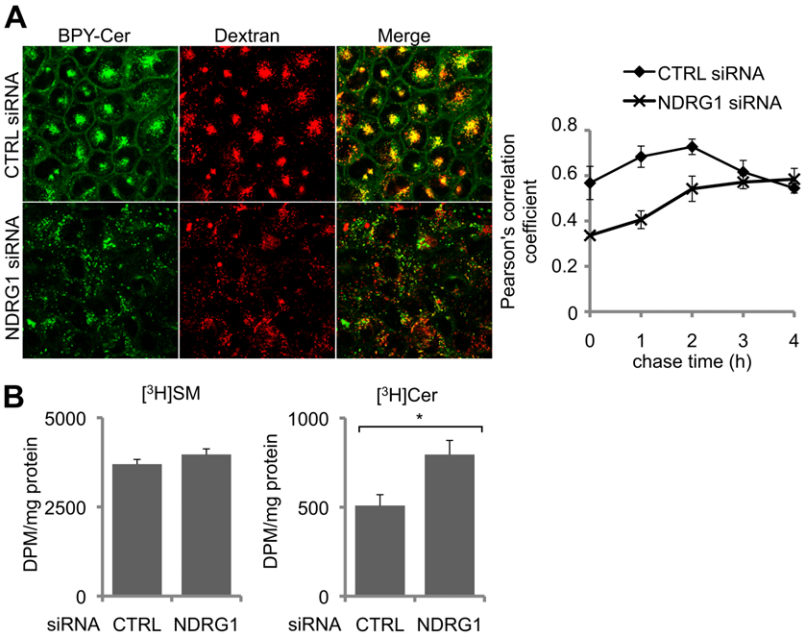

Fig. 6. Ceramide is enriched in enlarged MVBs in NDRG1 knockdown cells. (**A**) Altered BODIPY-labeled ceramide (BPY-Cer) transport in NDRG1-silenced cells. Cells pre-labeled with dextran were pulse-labeled with BPY-Cer/LDL for 1 hour and chased for 0–4 hours (images from 1 hour chase). Colocalization of BPY-Cer (green) and dextran (red) was analyzed using Pearson's correlation coefficient at 0–4 hours of chase. $n=3$ confocal sections and >30 cells per time point; values are means ± s.e.m. (**B**) [^{3}H]Ceramide accumulation derives from endosomal SM hydrolysis in NDRG1-silenced cells. [^{3}H]SM incorporated into LDL particles was internalized into A431 cells for 2 hours and the amounts of [^{3}H]SM and derived [^{3}H]ceramide were analyzed by TLC. Values are means ± s.e.m. of six samples/condition from two independent experiments, $*P<0.05$ (Student's t-test).

depletion could rescue the LDLR levels at the PM and reverse the endosomal LDLR accumulation in NDRG1-depleted cells. As expected, silencing of IDOL led to an increase in both total and PM LDLR abundance (Fig. 7C). Remarkably, depletion of IDOL in NDRG1 k/d cells was able to reverse the decrease in LDLR PM levels (Fig. 7C). Furthermore, under these conditions, depletion of IDOL alleviated the endosomal sequestration of LDLR (Fig. 7D). We also assessed the consequence of IDOL silencing on cellular cholesterol stores. Silencing of IDOL resulted in increased CES, whereas silencing of NDRG1 led to the opposite outcome (Fig. 7E). Strikingly, when IDOL and NDRG1 were silenced simultaneously, the level of CEs was rescued (Fig. 7E).

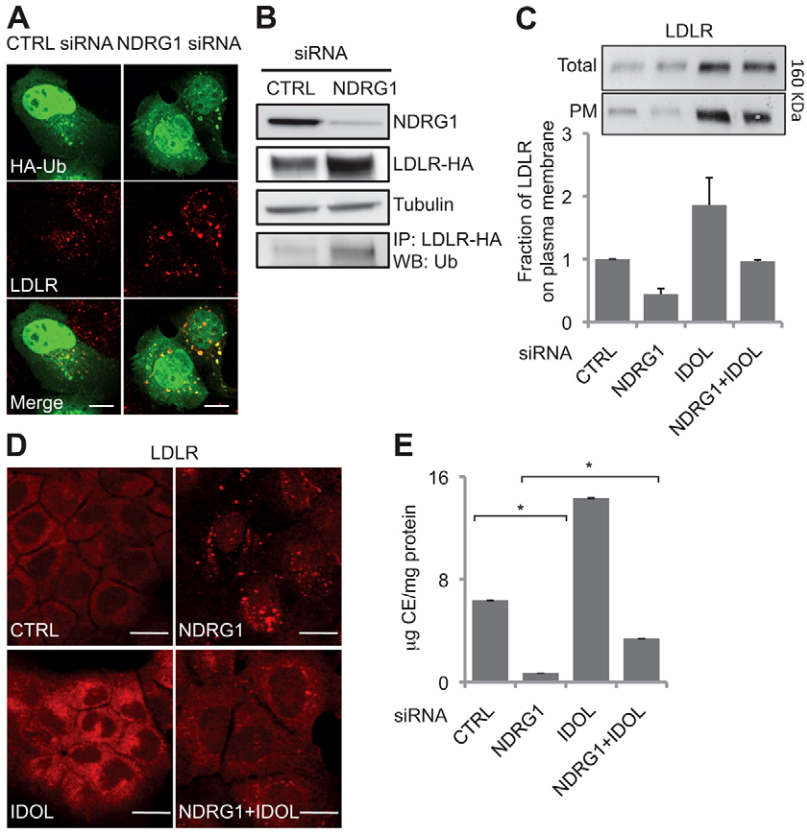

Fig. 7. LDLR ubiquitylation is increased in NDRG1-silenced cells, and its prevention by IDOL depletion rescues LDLR distribution and CE content. (**A**) LDLR colocalizes with HA–Ub in NDRG1-depleted cells. A431 cells were transfected with siRNAs and a plasmid encoding HA–Ub. HA–Ub was immunostained with anti-HA antibodies (green) and LDLR with anti-LDLR antibodies (red). Confocal microscopy images are shown. Scale bars: 10 µm. (**B**) LDLR is heavily ubiquitylated upon NDRG1 k/d. HEK293T cells were co-transfected with LDLR-HA and siRNAs and immunoblotted as indicated. LDLR–HA was immunoprecipitated from total cell lysates using HA-beads and the ubiquitylated LDLR–HA was detected with an anti-Ub antibody; α-tubulin was used as a loading control. A representative immunoblot of three independent experiments with comparable results is shown. (**C**) IDOL k/d rescues the PM localization of LDLR in NDRG1-silenced cells. siRNA-transfected A431 cells were analyzed by surface biotinylation as in Fig. 2B. Values are means ± s.e.m. of two independent experiments; a representative immunoblot is shown. (**D**) Depletion of IDOL in NDRG1-silenced cells complements the endosomal LDLR accumulation. siRNA-transfected A431 cells were permeabilized with filipin, immunostained with anti-LDLR antibody and imaged by confocal microscopy, using a 40× objective. Scale bars: 20 µm. (**E**) Depletion of IDOL in NDRG1-silenced cells rescues cellular CE content. To determine the CEs in siRNA-treated cells, lipids were extracted, separated by TLC, and quantified by densitometry. Values are means ± s.e.m., $*P<0.05$ (Student's t-test).

Taken together, these results demonstrate that LDLR is ubiquitylated in NDRG1-depleted cells and accumulates in abnormal enlarged endosomes/MVBs. If LDLR ubiquitylation in these cells is prevented, the receptor is not similarly sequestered in endosomes but can apparently recycle to the PM to rescue LDLR PM levels and LDL uptake. Accordingly, the cholesterol content of NDRG1-depleted cells is rescued.

NDRG1-depletion reduces glial cell LDL uptake and decreases the amount of Olig2 in an Idol-dependent manner

NDRG1 is highly expressed in myelinating glial cells (Okuda et al., 2008) and *NDRG1* mutations cause CMT4D. The major CMT4D-causing founder mutation of NDRG1 contains a premature termination signal at residue 148 (R148X) (Kalaydjieva et al., 2000). The *Ndrg1*$^{-/-}$ mice display a progressive demyelinating disorder, providing evidence that NDRG1 deficiency accounts for the disease (Okuda et al., 2004). Accordingly, we observed that although the overexpression of WT NDRG1 rescued the LDLR accumulation in NDRG1 k/d cells (supplementary material Fig. S6), a construct of NDRG1 truncated at R148 was unstable and was unable to rescue the phenotype (V. P. and E. I., unpublished observations). These data suggest that the effects of NDRG1 silencing might mimic the effects of functional NDRG1 deficiency in CMT4D.

We therefore studied the role of Ndrg1 in regulating LDL uptake in murine Oli-neu cells, a widely used oligodendroglial cell line generated by immortalization of mitotic oligodendrocyte precursor cells by retroviral *t-neu* oncogene expression (Jung et al., 1995). Silencing of Ndrg1 in Oli-neu cells (see supplementary material Fig. S1D) reduced DiI–LDL binding and uptake (Fig. 8A), analogously to our observations in A431 cells. In line with the effect of IDOL in other cell types, silencing of Idol in Oli-neu cells resulted in an increase in both DiI–LDL binding and uptake (Fig. 8A). Furthermore, depletion of Idol in Ndrg1-silenced cells re-established DiI–LDL binding and uptake to the level of control-siRNA-treated cells (Fig. 8A). These results suggest that Ndrg1 and Idol are involved in LDL uptake in oligodendrocytes and that these processes are interconnected.

Light microscopy revealed that control-siRNA-treated Oli-neu cells exhibited outgrowths characteristic of oligodendrocytes, whereas the Ndrg1-depleted cells had a distinct, spindle-shaped morphology. To quantify the number of outgrowths, control and Ndrg1-siRNA-treated cells were transfected with an expression plasmid encoding a constitutively farnesylated GFP construct (GFP-F). This construct localizes to the PM and enables visualization of neurite outgrowths (Lalli and Hall, 2005). The Ndrg1-depleted cells had fewer outgrowths per cell than control cells (Fig. 8B). A possible explanation is that the silencing of Ndrg1 affects the differentiation of Oli-neu cells. To test this idea, we immunoblotted and immunostained siRNA-transfected Oli-neu cells with an antibody against oligodendrocyte lineage transcription factor 2 (Olig2). Olig2 is necessary for the genesis of oligodendrocytes and is an important regulator of oligodendrocyte differentiation and myelination (Ligon et al., 2006). In Ndrg1-depleted cells Olig2 immunoreactivity was significantly reduced (~50%, based on immunoblotting; Fig. 8C) and the remaining Olig2 protein was largely cytoplasmic, in contrast to control cells that showed a strong nuclear Olig2 localization (V.P. and E.I., unpublished observations).

Finally, we examined the potential connection of oligodendrocyte differentiation and LDLR regulation by analyzing Olig2 levels after Idol k/d. Depletion of Idol slightly increased Olig2 protein levels. Importantly, Idol co-depletion in Ndrg1-silenced cells was able to rescue the reduced Olig2 levels (Fig. 8C). Cumulatively, these findings suggest that NDRG1 is

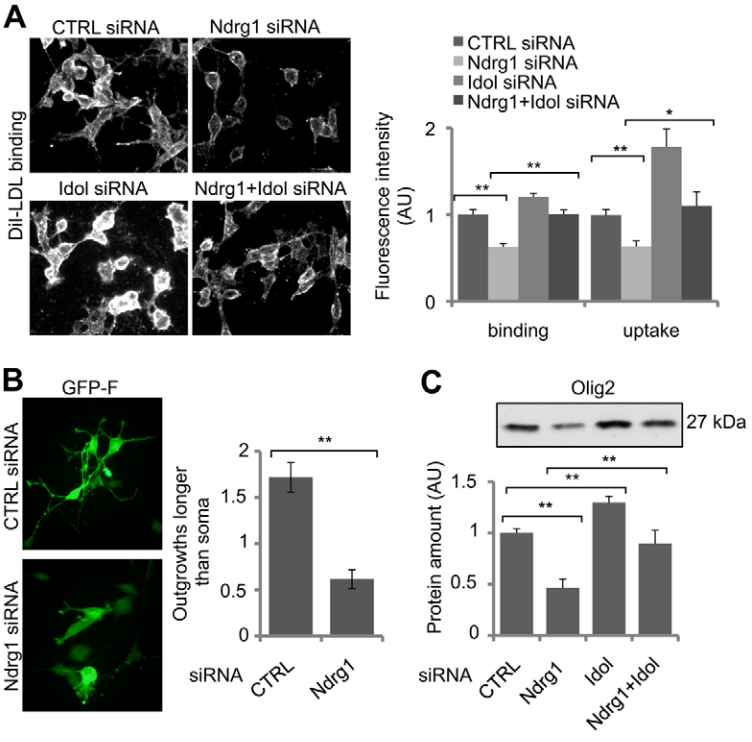

Fig. 8. Ndrg1 knockdown in murine oligodendrocytes results in reduced LDL uptake and decreases the amount of Olig2. (**A**) DiI–LDL binding and uptake are reduced in Ndrg1-silenced Oli-neu cells. Cells were incubated with 2 µg/ml DiI–LDL for 20 minutes at 4℃ (binding) or for 30 minutes at 37℃ (uptake). Cells were imaged and the fluorescence intensity per cell was quantified. Values are means ± s.e.m. of two to four independent experiments (at least 900 cells analyzed/condition); $^{**}P<0.001$, $^{*}P<0.05$ (Student's *t*-test). (**B**) Number of Oli-neu cell outgrowths is diminished upon Ndrg1 k/d. A plasmid encoding GFP-F was transfected to siRNA-treated Oli-neu cells to visualize and quantify outgrowths. Values are mean ± s.e.m., 50 cells/condition, $^{**}P<0.001$ (Student's *t*-test). (**C**) Ndrg1 silencing leads to a reduction in the amount of Olig2 but co-depletion of Idol complements the phenotype. Oli-neu cells were collected after 72 hours of siRNA transfection and Olig2 protein amounts were analyzed by western blotting and quantified by densitometry. Values are means ± s.e.m. of four experiments, $^{**}P<0.001$ (Student's *t*-test).

important for oligodendrocyte cholesterol balance and differentiation and that these actions might be mediated through IDOL-sensitive LDLR family members (Hong et al., 2010).

Discussion

NDRG1 as a regulator of LDLR trafficking

When cells are in need of cholesterol, the endocytosed LDLR normally recycles rapidly to the PM (Goldstein and Brown, 2009). We found that in NDRG1-depleted cells, the receptor was reduced at the cell surface and accumulated in modified early endosomes and MVBs. In parallel, the degradation of LDLR was slowed down, contributing to an increase in the total cellular LDLR. The decreased LDLR degradation is in agreement with the fact that a functional MVB pathway is needed for lysosome biogenesis and is essential for cargo degradation (Mukhopadhyay and Riezman, 2007).

LDLR ubiquitylation by IDOL is known to act as a sorting signal that directs the receptor for lysosomal degradation (Hong et al., 2010; Zelcer et al., 2009). Our findings indicate that the LDLR in NDRG1-depleted cells is heavily ubiquitylated, suggesting that it is targeted for lysosomal degradation. We propose that the LDLR must be ubiquitylated by IDOL in order to be sequestered into the abnormal endosomal compartment observed in NDRG1-deficient cells. In line with this, LDLR is able to recycle to the PM in the simultaneous absence of IDOL and NDRG1. This recycling LDLR is likely to utilize distinct endosomal subpopulations or subdomains from those involved in MVB formation and eventual cargo degradation. Indeed, endosomes are known to exist in cargo-specific populations (Lakadamyali et al., 2006) and cargo-specific signals can modify the endosomal pathway (Miaczynska et al., 2004; van der Goot and Gruenberg, 2006).

NDRG1 as a regulator of endosomal morphology and function

The enlarged MVBs in NDRG1 k/d cells contained more intraluminal vesicles, suggesting that the mechanism(s) of intraluminal vesicle formation and/or turnover were altered upon NDRG1 depletion. These atypical MVBs sequestered recycling membrane proteins, such as the LDLR. Of note, they also accumulate the transferrin receptor, E-cadherin (Kachhap et al., 2007), and β1-integrin (V. P. and E. I., unpublished observations). In addition, they accumulated lipids (free cholesterol and ceramide) and ubiquitin, and were positive for EEA1. The mechanisms by which the enlarged MVBs and increased number of intraluminal vesicles are generated upon NDRG1 k/d might involve several mechanisms. Based on earlier studies and our observations these mechanisms could include: (1) altered activity of endosomal Rab GTPases (Huotari and Helenius, 2011); (2) downregulation of ESCRT complex components (Stuffers et al., 2009); (3) increased cholesterol/ceramide content in MVBs (Kobuna et al., 2010; Trajkovic et al., 2008); (4) increased ubiquitylation of cargo (MacDonald et al., 2012); and (5) decreased degradation of cargo (Huotari and Helenius, 2011).

The biogenesis of the atypical MVBs in NDRG1 k/d cells was accompanied by diminished amounts of PRA1 and ESCRT complex components. Of PRA1, about two-thirds was depleted upon NDRG1 silencing. PRA1 has been shown to interact with NDRG1 and regulate several endosomal Rab GTPases, including Rabs 4, 5, 7 and 9 (Bucci et al., 1999; Sivars et al., 2003), and to affect the endosomal cholesterol content (Liu et al., 2011). Moreover, we found that PRA1 overexpression alleviates the LDLR redistribution in NDRG1-silenced cells. Therefore, the shortage of PRA1 in NDRG1-silenced cells might alter the delivery of Rab GTPases to endosomal membranes (Sivars et al., 2003), thereby contributing to the disturbed endosomal morphology and membrane transport.

Interestingly, our data indicate that MVB biogenesis and endosomal concentration of ubiquitylated cargo can proceed in NDRG1-depleted cells despite downregulation of ESCRT proteins. Although ESCRT-independent mechanisms for MVB formation have been proposed (Stuffers et al., 2009; Trajkovic et al., 2008), the physiological regulators of this process remain largely unknown. We suggest that in NDRG1-silenced cells, the endosomal accumulation of ceramide (presumably deriving from SM hydrolysis) triggers the formation of intraluminal vesicles. As such, NDRG1 appears as the first protein to negatively regulate the formation of ceramide-rich intraluminal vesicles. In future studies, it will be important to elucidate in more detail how NDRG1 could control this process.

NDRG1 and CMT4D

To extend our findings to a pathophysiologically relevant cell model, we studied glial cells. We show that in rodent oligodendrocytes, which normally exhibit strong Ndrg1 expression in the cytoplasm and processes (Berger et al., 2004; Okuda et al., 2008), Ndrg1 deficiency results in reduced LDL uptake. Importantly, this implies that the NDRG1 effect on LDL uptake is not specific for a certain cell type or species. High cholesterol availability is known to be required for myelin membrane growth (Saher et al., 2005). In addition, studies in other CMT neuropathies have emphasized the importance of endocytic pathways in the formation of myelin (Lee et al., 2012; Roberts et al., 2010; Sidiropoulos et al., 2012; Stendel et al., 2010; Verhoeven et al., 2003), reinforcing a link between NDRG1 function in endocytic trafficking and myelin formation/maintenance.

NDRG1 might also affect oligodendrocyte differentiation, as suggested by the lack of outgrowths and downregulation of Olig2 in Ndrg1-silenced oligodendrocytes. This agrees with the notion that the NDRG1 transcript is strongly upregulated during oligodendrocyte differentiation (Cahoy et al., 2008). We describe for the first time that Idol is involved in the regulation of lipid uptake in oligodendroglial cells. This finding is consistent with a recent report showing that liver X receptors (LXRs) that are transcriptional regulators of Idol expression control lipid metabolism in this cell type (Nelissen et al., 2012).

Intriguingly, IDOL not only promotes the ubiquitylation of the LDLR (Zelcer et al., 2009) but also two related receptors, the ApoE receptor 2 (ApoER2) and very-low-density lipoprotein receptor (VLDLR) (Hong et al., 2010), known to be expressed in oligodendrocytes (Zhao et al., 2007). Indeed, a potential explanation for the rescue of Olig2 levels by Idol depletion in Ndrg1 k/d cells is that uptake of LDL, or other ligands of IDOL-regulated receptors, is required to maintain Olig2 expression and oligodendrocyte differentiation. Notably, both ApoER2 and VLDLR have been shown to mediate Idol-sensitive Reelin signaling (Hong et al., 2010), a pathway crucial for the proper development of the nervous system. Moreover, Olig2-expressing oligodendroglial precursor cells are absent in mice lacking

megalin, another LDLR family member involved in the endocytosis of multiple ligands (Wicher and Aldskogius, 2008).

In summary, this study identifies NDRG1 as a novel regulator of MVB integrity and LDLR endosomal recycling. In the absence of this protein, ubiquitylated LDLR accumulates in modified early endosomes/MVBs that harbor increased amounts of ceramide-rich intraluminal vesicles. Thus, NDRG1 emerges as a critical protein that stimulates receptor recycling and limits the number of intraluminal vesicles in MVBs. Exactly how NDRG1 co-operates with known regulators of this process, such as ESCRT components and Rab GTPases, and how broadly NDRG1 regulates recycling membrane proteins, remain to be addressed. Importantly, the regulatory function of NDRG1 in endosomal dynamics appears to hold for several cell systems; therefore, it is likely to be relevant for understanding the contribution of NDRG1 both in neuropathy and in tumorigenesis.

Materials and Methods

Antibodies and other reagents

The following antibodies were used: NDRG1 (rabbit pAb; T. Commes, Universite Montpellier, France), NDRG1 (rabbit pAb; Atlas Antibodies AB, Stockholm, Sweden), LDLR (mAb C7, mouse hybridoma supernatant; Beisiegel et al., 1981; immunostainings), LDLR (rabbit pAb, 20R-LR002, Fitzgerald Industries International, Acton, Massachusetts, USA; immunostainings and western blotting), LDLR (rabbit mAb, clone EP1553Y, Epitomics, Burlingame, CA, USA; western blotting), LAMP1 (mAb H4A3, Developmental Studies Hybridoma Bank, Iowa, Maryland, USA), EEA1 (mAb, BD Biosciences, San Jose, CA, USA), PRA1 (mAb 2A4, Novus Biologicals, Littleton, Colorado, USA), TSG101 (mAb 4A10, GeneTex Inc., Irvine, CA, USA), ubiquitin (mAb FK2, BML-PW8810, Enzo Life Sciences, Farmingdale, New York, USA), hemagglutinin (HA) (mAb, Sigma-Aldrich, St. Louis, MO, USA), β-tubulin (mAb, T4026, Sigma-Aldrich), α-tubulin (mAb, T9026/clone DM1A, Sigma) and Hrs, Vps22, Vps24 and Vps32 rabbit pAbs (H. Stenmark). U81666A [3β-(2-diethylaminoethoxy)androst-5-en-17-one], HPLC-grade solvents, lovastatin, and silica gel 60 TLC plates were from Merck (Darmstadt, Germany), [1,2-^{3}H]cholesterol from Perkin Elmer (Waltham, MA), [^{3}H]acetic acid from GE Healthcare (Chalfont St. Giles, UK), dextran–Alexa-Fluor-568 (10000MW) and DiI–LDL from Invitrogen-Life Technologies (Carlsbad, California, USA), Effectene and Hiperfect from Qiagen (Germantown, Maryland, USA), protease inhibitors (chymostatin, leupeptin, antipain and pepstatin A), Triton X-100, filipin and mevalonic acid lactone (mevalonate) from Sigma-Aldrich and diethyl ether and petroleum ether from J. T. Baker (Avantor Performance Materials, Center Valley, Pennsylvania, USA). For electron microscopy, glutaraldehyde and osmium tetroxide were purchased from Electron Microscopical Sciences (Hatfield, Pennsylvania, USA) and sodium cacodylate and potassium ferrocyanide were from Sigma-Aldrich. D-erythro-*N*-palmitoyl-BODIPY-sphingosine (Ceramide-BDY) was prepared by *N*-acylation of BODIPY–sphingosine, as described by Blom et al. (Blom et al., 2012). All cell culture reagents, except poly-D-lysine (Sigma-Aldrich), were obtained from Gibco Life Technologies (Invitrogen). Lipoprotein-deficient serum (LPDS) was prepared as described previously (Jansen et al., 2008).

Plasmid and siRNA transfections

Human PRA1 cDNA (NM_006423.1) in pCMV6-XL5 was purchased from Origene (Rockville, Maryland, USA). The LDLR-HA and HA-ubiquitin plasmids have been previously described (Hong et al., 2010; Zelcer et al., 2009). The following siRNAs were used: CTRL (Sigma-Aldrich; 5′-CGUAC-GCGGAAUACUUCGA-3′), human NDRG1 (Stealth-modified, Invitrogen; 5′-CAUCGAGACUUUACAUGGCUCUGUU-3′), mouse Ndrg1 (Qiagen FlexiTube, target sequence 5′-AACTCATTCCTGGAAACAAA-3′), human IDOL (s26522, Ambion Silencer Select, Invitrogen; 5′-GACUUUAGCCCAAUUAAUATT-3′), mouse Idol-6 (Ambion Silencer Select, Invitrogen; target sequence 5′-AA-CATTAACCTTGGTAAGAAA-3′), mouse Idol-9 (Ambion Silencer Select, Invitrogen; target sequence 5′-AGGGATCATCGAGGTTGATTA-3′), Rab4a (Qiagen validated, 5′-AAUGCAGGAACUGGCAAAUCT-3′) and PRA1 (Kim et al., 2006) (Stealth-modified, Invitrogen, 5′-GCGCCUGUUACAUUC-UCUAUCUGCG-3′). TSG101 and Hrs siRNAs have been previously described (Bache et al., 2003; Garrus et al., 2001). cDNA transfections were performed with Effectene and siRNA transfections in 10 nM final concentration with HiPerfect according to the manufacturer's instructions. To silence mouse Idol, two different siRNAs (Idol-6 and −9) were used (total 10 nM final concentration). In co-silencing experiments of two different genes, each siRNA was used at 10 nM. The siRNA transfection time was 72 hours unless otherwise stated.

Cell culture and western blot analysis

A431 cells (epidermoid carcinoma cell line, American Type Culture Collection; ATCC) and HEK293T cells (human embryonic kidney cells, ATCC) were cultured in Dulbecco's modified Eagle's medium (D-MEM) supplemented with 10% fetal bovine serum, 0.5 mM L-glutamine and 100 IU/ml penicillin, 100 µg/ml streptomycin at 37℃ in a CO_2-conditioned, humidified incubator. Oli-neu, an immortalized oligodendrocyte precursor cell line (Jung et al., 1995) was cultured in 1:1 D-MEM/HAM's F12 with B27 supplement on poly-D-lysine (50 µg/ml)-coated plastic. Cells were treated with U18666A (48 hours) in 10% FBS or loaded with LDL (18 hours) in 5% LPDS. Cells were collected for western blotting by adding 1% NP-40 including a protease inhibitor mixture (chymostatin, leupeptin, antipain and pepstatin A; 25 µg/ml each; CLAP) in PBS. The protein amount was determined by using a BioRad kit. Proteins were subjected to SDS-PAGE and western blotting as described (Jansen et al., 2008). In some experiments, the IRDye-conjugated secondary antibodies (IRDye 800CW-conjugated donkey anti-rabbit and 680LT donkey anti-mouse, LI-COR, Superior St. Lincoln, Nebraska, USA) were used prior to image capture with Odyssey Imager (LI-COR). Immunoreactive bands were quantified using ImageJ software (National Institutes of Health, Bethesda, Maryland, USA; NIH, http://rsbweb.nih.gov/ij/).

Immunofluorescence staining

Cells were fixed with 4% paraformaldehyde for 20 minutes at room temperature, and permeabilized with 0.1% or 0.3% Triton X-100 for 5 minutes. For visualization of free cholesterol, cells were stained with 0.05% filipin in 10% FBS–PBS blocking solution for 30 minutes at 37℃. The immunostainings were performed sequentially as described by Jansen et al. (Jansen et al., 2008). Images were acquired with an Olympus AX70 epifluorescence microscope (Olympus, Center Valley, Pennsylvania, USA) equipped with an Olympus DP71 CCD camera, using 20× or 40× objectives. Confocal images were acquired with a Leica TCS SP2 AOBS confocal microscope (Leica Microsystems, Wetzlar, Germany), with 40× (NA=1.25) or 60× (NA=1.4) oil objectives.

Biochemical lipid analyses

siRNA-transfected A431 cells were collected in 0.2 N NaOH and lipids were extracted as described previously (Bligh and Dyer, 1959). FC and CE were resolved on TLC plates using hexane/diethyl ether/acetic acid (80:20:1) as the mobile phase. Lipids were visualized by charring and quantified by ImageJ after scanning. To measure cholesterol synthesis, cells were pulse-labeled in serum-free medium with 20 µCi/ml [^{3}H]acetic acid in six-well plates for 2 hours at 37℃, chased for 2 hours in serum-free medium with 10 mM lovastatin and 2.5 mM mevalonate, and analyzed as described previously (Heino et al., 2000). For analysis of cholesterol efflux, [^{3}H]cholesterol (2 µCi/ml) was added to A431 cells 24 hours after siRNA transfection, the cells were incubated for an additional 8 hours, and then for 16 hours in serum-free medium in the presence of ApoA-I (10 µg/ml). The medium was collected, cells were scraped into ice-cold PBS, harvested by centrifugation and resuspended in 0.2 N NaOH. The radioactivity in medium and cells was measured by scintillation counting.

DiI–LDL binding and uptake

siRNA-transfected A431 and Oli-neu cells on coverslips were incubated with 5 µg/ml (A431 cells) or 2 µg/ml (Oli-neu cells) of DiI–LDL for 30 minutes at 4℃ (binding) or 20–30 minutes at 37℃ (uptake) in serum-free medium prior to fixation with 4% PFA and staining with DAPI for detection of the nuclei. The samples were imaged with an Olympus AX70 microscope to quantify DiI–LDL intensity. The total intensity obtained from background-substracted DiI–LDL images was divided by the number of nuclei in the image to obtain an intensity-per-cell value. Alternatively, cells were plated onto 48-well plates, transfected with siRNAs and incubated with DiI–LDL as above. Cells were washed three times with PBS prior to lysis into 200 µl of PBS–1% NP-40. The lysates were incubated on ice for 10 minutes, and 150 µl aliquots were measured in a PheraStar microplate reader (BMG Labtech, Ortenberg, Germany) with an ex540/em590 filter set. Fluorescence counts were normalized to total protein (determined from 10 µl aliquots).

Cell surface biotinylation and LDLR degradation

Cell surface biotinylation protocol was modified from Scotti et al. (Scotti et al., 2011). Cells on 60 mm plates were rinsed twice with ice-cold PBS containing 0.02 mM $CaCl_2$ and 0.15 mM $MgCl_2$ (PBS+). Cell surface proteins were biotinylated for 20 minutes with 0.5 mg/ml biotin (Sulfo-NHS-LC-Biotin; Pierce/Thermo Fisher Scientific, Rockford, Illinois, USA) diluted in PBS+. Unbound biotin was quenched by two incubations (5 minutes at 4℃) with PBS+ containing 0.1 M glycine and 0.3% BSA. The cells were washed with PBS+ and lysed (10 minutes at 4℃) in 300 µl lysis buffer (0.2% SDS, 2% NP-40 in PBS, supplemented with protease inhibitors). Lysates were collected and cleared by centrifugation, and an aliquot (20 µl) was taken for immunoblotting with the LDL receptor antibody ('total'). Biotinylated proteins from the rest of the lysate (250 µl) were precipitated with 50 µl streptavidin–agarose beads (Sigma-Aldrich)

by rotation overnight at 4℃. The beads were washed three times in cold lysis buffer and twice in PBS+. Biotinylated proteins were eluted from the beads by boiling in 2× sample buffer, separated by SDS-PAGE, and transferred to nitrocellulose for western blotting. Blots were quantified by densitometry using ImageJ. To quantify LDLR degradation, the cell surface was biotinylated and quenched as above. The cells were washed in PBS+ and chased for 0, 2, or 5 hours in complete culture medium at 37℃, lysed, and the biotinylated proteins were precipitated and LDLR amounts detected as described above.

Quantification of LDLR accumulation

Cells were transfected with control or NDRG1 siRNAs as described above and with PRA1 or pEGFP cDNA 48 hours later. At day 3, cells were fixed with 4% PFA and stained with anti-PRA1 and anti-LDLR antibodies. The number of intracellular LDLR-positive accumulations was quantified from Leica confocal images in ImageJ by counting the local maxima of the region of interest (ROI), using the 'Find maxima' plugin filter of ImageJ (http://rsbweb.nih.gov/ij/docs/menus/process.html). Cells expressing the transfected constructs (PRA1 or GFP) were defined as ROIs, and maxima were scored as 'LDLR-positive accumulations'.

Electron microscopy

Cells were cultured on glass coverslips, fixed with 2.5% glutaraldehyde in 0.1 M sodium cacodylate buffer, post-fixed with 1% osmium tetroxide and 1.5% potassium ferrocyanide and dehydrated. A plastic capsule filled with embedding resin was inverted over the coverslip. After polymerization the coverslip was removed and the cells were sectioned horizontally. MVBs were systematically sampled to give a total of 60 MVBs from two individual experiments in each group, and the diameter of MVBs and number of intraluminal vesicles in the plane of sectioning were assessed in prints with a final magnification of 145000×. BSA–16 nm colloidal gold complexes were prepared according to the method of Griffiths (Griffiths, 1993). Cells were incubated with BSA–gold (OD_{520}=1) in Hepes-buffered D-MEM for 40 minutes at 37℃, fixed and processed as described above.

Ceramide quantification

Cells were washed with PBS and scraped into 800 µl of ice cold 2% NaCl. Aliquots (5 µl) were removed for protein determination. Then, 3 ml $CHCl_3$/methanol (2:1) was added, the suspension was vortexed, 1 ml of $CHCl_3$ and 1 ml of H_2O were added for phase separation, and the lower phase was collected. Lipid extracts were dried under a stream of nitrogen, lipids were re-dissolved in $CHCl_3$/methanol (2:1), and resolved with known standards on HPTLC plates with $CHCl_3$:acetic acid (9:1) as the mobile phase. HPTLC plates were dried, dipped in 3% $CuSO_4$/8% H_3PO_4, and the ceramide bands were visualized by charring with H_2SO_4 in ethanol at 180℃.

Metabolism of LDL-derived [^{3}H]SM cells was measured as previously described (Blom et al., 2012). In brief, cells were serum-starved overnight and then incubated with 50 µg/ml [^{3}H]SM/LDL for 2 hours. Cellular lipids were extracted and separated on HPTLC. Bands corresponding to lipid standards were scraped and measured by scintillation counting.

BODIPY-Cer trafficking

LDL particles were labeled with BODIPY-Cer according to (Blom et al., 2012). Cells were labeled overnight with Alexa-Fluor-568–dextran in medium containing 5% LPDS, incubated for an additional 2 hours in the absence of dextran (to chase dextran to lysosomes) and then labeled with 50 µg/ml BODIPY–Cer/LDL for 1 hours. The cells were washed and imaged by confocal microscopy at 37℃ for 4 hours. Colocalization of BODIPY-labeled ceramide and dextran was quantified using Pearson's correlation coefficient.

Immunoprecipitation of ubiquitylated proteins

Immunoprecipitation of HA-tagged proteins was performed as previously described (Zelcer et al., 2009). Briefly, equal amounts of protein in the cleared lysates were incubated with EZview^{TM} red anti-HA affinity beads (Sigma-Aldrich) for 16 hours. Subsequently, beads were washed 4× with RIPA buffer. All incubations and washes were performed at 4℃ with rotation. Proteins were eluted from the beads by boiling in 1× protein sample buffer for 5 minutes prior to western blotting and quantification.

Acknowledgements

We thank A. Uro and P. Kaipainen (University of Helsinki, Finland) for excellent technical help, and T. Commes (Université Montpellier, France), M. Carducci (Johns Hopkins University, USA), H. Stenmark (Oslo University Hospital, Norway), Peter van der Sluijs (University Medical Center Utrecht, Utrecht, Netherlands) and M. Simons (Max-Planck Institute of Experimental Medicine, Göttingen, Germany) for kindly providing the anti-NDRG1 antibody, NDRG1-Flag construct, ESCRT antibodies, Rab4 antibody and Oli-neu cells, respectively. We thank the Biomedicum Imaging Unit and the Electron Microscopy Unit of the Institute of Biotechnology, University of Helsinki, for facilities.

Author contributions

V.P., N.Z. and E.I. designed the experiments. V.P., B.V., T.B., W.W., J.N. and N.B. performed and analyzed the experiments. R.B. provided reagents. V.P., B.V., R.B., N.Z. and E.I. wrote the manuscript.

Funding

This study was supported by the Finnish Medical Foundation, Academy of Finland [grant numbers 1117064 to V.P., 131429, 131489 to E.I.]; a University of Helsinki postdoctoral researcher grant (to V.P.), the Kymenlaakso Cultural Foundation (to V.P.); the Georg and Ella Ehrnrooth Foundation; the Magnus Ehrnrooth Foundation; the Liv och Hälsa Foundation; a Career Development award from the Human Frontier Science Program Organization [grant number CDA-00057/2009 to N.Z.]; and a VIDI grant from the Netherlands Organization of Scientific Research [grant number 017.106.355 to N.Z.].

Supplementary material available online at
http://jcs.biologists.org/lookup/suppl/doi:10.1242/jcs.128132/-/DC1

References

Bache, K. G., Raiborg, C., Mehlum, A. and Stenmark, H. (2003). STAM and Hrs are subunits of a multivalent ubiquitin-binding complex on early endosomes. *J. Biol. Chem.* **278**, 12513-12521.

Bandyopadhyay, S., Pai, S. K., Gross, S. C., Hirota, S., Hosobe, S., Miura, K., Saito, K., Commes, T., Hayashi, S., Watabe, M. et al. (2003). The Drg-1 gene suppresses tumor metastasis in prostate cancer. *Cancer Res.* **63**, 1731-1736.

Bartz, F., Kern, L., Erz, D., Zhu, M., Gilbert, D., Meinhof, T., Wirkner, U., Erfle, H., Muckenthaler, M., Pepperkok, R. et al. (2009). Identification of cholesterol-regulating genes by targeted RNAi screening. *Cell Metab.* **10**, 63-75.

Beisiegel, U., Schneider, W. J., Goldstein, J. L., Anderson, R. G. and Brown, M. S. (1981). Monoclonal antibodies to the low density lipoprotein receptor as probes for study of receptor-mediated endocytosis and the genetics of familial hypercholesterolemia. *J. Biol. Chem.* **256**, 11923-11931.

Berger, P., Sirkowski, E. E., Scherer, S. S. and Suter, U. (2004). Expression analysis of the N-Myc downstream-regulated gene 1 indicates that myelinating Schwann cells are the primary disease target in hereditary motor and sensory neuropathy-Lom. *Neurobiol. Dis.* **17**, 290-299.

Bligh, E. G. and Dyer, W. J. (1959). A rapid method of total lipid extraction and purification. *Can. J. Biochem. Physiol.* **37**, 911-917.

Blom, T., Li, Z., Bittman, R., Somerharju, P. and Ikonen, E. (2012). Tracking sphingosine metabolism and transport in sphingolipidoses: NPC1 deficiency as a test case. *Traffic* **13**, 1234-1243.

Bucci, C., Chiariello, M., Lattero, D., Maiorano, M. and Bruni, C. B. (1999). Interaction cloning and characterization of the cDNA encoding the human prenylated rab acceptor (PRA1). *Biochem. Biophys. Res. Commun.* **258**, 657-662.

Cahoy, J. D., Emery, B., Kaushal, A., Foo, L. C., Zamanian, J. L., Christopherson, K. S., Xing, Y., Lubischer, J. L., Krieg, P. A., Krupenko, S. A. et al. (2008). A transcriptome database for astrocytes, neurons, and oligodendrocytes: a new resource for understanding brain development and function. *J. Neurosci.* **28**, 264-278.

Carstea, E. D., Morris, J. A., Coleman, K. G., Loftus, S. K., Zhang, D., Cummings, C., Gu, J., Rosenfeld, M. A., Pavan, W. J., Krizman, D. B. et al. (1997). Niemann-Pick C1 disease gene: homology to mediators of cholesterol homeostasis. *Science* **277**, 228-231.

Echaniz-Laguna, A., Degos, B., Bonnet, C., Latour, P., Hamadouche, T., Lévy, N. and Leheup, B. (2007). NDRG1-linked Charcot-Marie-Tooth disease (CMT4D) with central nervous system involvement. *Neuromuscul. Disord.* **17**, 163-168.

Garrus, J. E., von Schwedler, U. K., Pornillos, O. W., Morham, S. G., Zavitz, K. H., Wang, H. E., Wettstein, D. A., Stray, K. M., Côté, M., Rich, R. L. et al. (2001). Tsg101 and the vacuolar protein sorting pathway are essential for HIV-1 budding. *Cell* **107**, 55-65.

Goldstein, J. L. and Brown, M. S. (2009). The LDL receptor. *Arterioscler. Thromb. Vasc. Biol.* **29**, 431-438.

Griffiths, G. (1993). *Fine Structure Immunohistochemistry*. Berlin: Springer-Verlag.

Guan, R. J., Ford, H. L., Fu, Y., Li, Y., Shaw, L. M. and Pardee, A. B. (2000). Drg-1 as a differentiation-related, putative metastatic suppressor gene in human colon cancer. *Cancer Res.* **60**, 749-755.

Heino, S., Lusa, S., Somerharju, P., Ehnholm, C., Olkkonen, V. M. and Ikonen, E. (2000). Dissecting the role of the golgi complex and lipid rafts in biosynthetic transport of cholesterol to the cell surface. *Proc. Natl. Acad. Sci. USA* **97**, 8375-8380.

Hölttä-Vuori, M., Vainio, S., Kauppi, M., Van Eck, M., Jokitalo, E. and Ikonen, E. (2012). Endosomal actin remodeling by coronin-1A controls lipoprotein uptake and degradation in macrophages. *Circ. Res.* **110**, 450-455.

Hong, C., Duit, S., Jalonen, P., Out, R., Scheer, L., Sorrentino, V., Boyadjian, R., Rodenburg, K. W., Foley, E., Korhonen, L. et al. (2010). The E3 ubiquitin ligase IDOL induces the degradation of the low density lipoprotein receptor family members VLDLR and ApoER2. *J. Biol. Chem.* **285**, 19720-19726.

Hunter, M., Angelicheva, D., Tournev, I., Ingley, E., Chan, D. C., Watts, G. F., Kremensky, I. and Kalaydjieva, L. (2005). NDRG1 interacts with APO A-I and A-II and is a functional candidate for the HDL-C QTL on 8q24. *Biochem. Biophys. Res. Commun.* **332**, 982-992.

Huotari, J. and Helenius, A. (2011). Endosome maturation. *EMBO J.* **30**, 3481-3500.

Ikonen, E. (2008). Cellular cholesterol trafficking and compartmentalization. *Nat. Rev. Mol. Cell Biol.* **9**, 125-138.

Jansen, M., Pietiaïnen, V. M., Pölönen, H., Rasilainen, L., Koivusalo, M., Ruotsalainen, U., Jokitalo, E. and Ikonen, E. (2008). Cholesterol substitution increases the structural heterogeneity of caveolae. *J. Biol. Chem.* **283**, 14610-14618.

Jung, M., Krämer, E., Grzenkowski, M., Tang, K., Blakemore, W., Aguzzi, A., Khazaie, K., Chlichlia, K., von Blankenfeld, G., Kettenmann, H. et al. (1995). Lines of murine oligodendroglial precursor cells immortalized by an activated neu tyrosine kinase show distinct degrees of interaction with axons in vitro and in vivo. *Eur. J. Neurosci.* **7**, 1245-1265.

Kachhap, S. K., Faith, D., Qian, D. Z., Shabbeer, S., Galloway, N. L., Pili, R., Denmeade, S. R., DeMarzo, A. M. and Carducci, M. A. (2007). The N-Myc down regulated Gene1 (NDRG1) Is a Rab4a effector involved in vesicular recycling of E-cadherin. *PLoS ONE* **2**, e844.

Kalaydjieva, L., Hallmayer, J., Chandler, D., Savov, A., Nikolova, A., Angelicheva, D., King, R. H., Ishpekova, B., Honeyman, K., Calafell, F. et al. (1996). Gene mapping in Gypsies identifies a novel demyelinating neuropathy on chromosome 8q24. *Nat. Genet.* **14**, 214-217.

Kalaydjieva, L., Nikolova, A., Turnev, I., Petrova, J., Hristova, A., Ishpekova, B., Petkova, I., Shmarov, A., Stancheva, S., Middleton, L. et al. (1998). Hereditary motor and sensory neuropathy—Lom, a novel demyelinating neuropathy associated with deafness in gypsies. Clinical, electrophysiological and nerve biopsy findings. *Brain* **121**, 399-408.

Kalaydjieva, L., Gresham, D., Gooding, R., Heather, L., Baas, F., de Jonge, R., Blechschmidt, K., Angelicheva, D., Chandler, D., Worsley, P. et al. (2000). N-myc downstream-regulated gene 1 is mutated in hereditary motor and sensory neuropathy-Lom. *Am. J. Hum. Genet.* **67**, 47-58.

Kim, J. T., Cho, M. Y., Choi, S. C., Kim, J. W., Chae, S. K., Yoon, D. Y., Kim, J. W. and Lim, J. S. (2006). Prenylated Rab acceptor 1 (PRA1) inhibits TCF/beta-catenin signaling by binding to beta-catenin. *Biochem. Biophys. Res. Commun.* **349**, 200-208.

Kim, J. T., Kim, J. W., Kang, Y. H., Kim, K. D., Lee, S. J., Choi, S. C., Kim, K. S., Chae, S. K., Kim, J. W., Lim, J. S. et al. (2012). NDRG2 and PRA1 interact and synergistically inhibit T-cell factor/β-catenin signaling. *FEBS Lett.* **586**, 3962-3968.

King, R. H., Chandler, D., Lopaticki, S., Huang, D., Blake, J., Muddle, J. R., Kilpatrick, T., Nourallah, M., Miyata, T., Okuda, T. et al. (2011). Ndrg1 in development and maintenance of the myelin sheath. *Neurobiol. Dis.* **42**, 368-380.

Ko, D. C., Gordon, M. D., Jin, J. Y. and Scott, M. P. (2001). Dynamic movements of organelles containing Niemann-Pick C1 protein: NPC1 involvement in late endocytic events. *Mol. Biol. Cell* **12**, 601-614.

Kobuna, H., Inoue, T., Shibata, M., Gengyo-Ando, K., Yamamoto, A., Mitani, S. and Arai, H. (2010). Multivesicular body formation requires OSBP-related proteins and cholesterol. *PLoS Genet.* **6**.

Lachat, P., Shaw, P., Gebhard, S., van Belzen, N., Chaubert, P. and Bosman, F. T. (2002). Expression of NDRG1, a differentiation-related gene, in human tissues. *Histochem. Cell Biol.* **118**, 399-408.

Lakadamyali, M., Rust, M. J. and Zhuang, X. (2006). Ligands for clathrin-mediated endocytosis are differentially sorted into distinct populations of early endosomes. *Cell* **124**, 997-1009.

Lalli, G. and Hall, A. (2005). Ral GTPases regulate neurite branching through GAP-43 and the exocyst complex. *J. Cell Biol.* **171**, 857-869.

Lee, S. M., Chin, L. S. and Li, L. (2012). Charcot-Marie-Tooth disease-linked protein SIMPLE functions with the ESCRT machinery in endosomal trafficking. *J. Cell Biol.* **199**, 799-816.

Ligon, K. L., Fancy, S. P., Franklin, R. J. and Rowitch, D. H. (2006). Olig gene function in CNS development and disease. *Glia* **54**, 1-10.

Liu, H. P., Wu, C. C., Kao, H. Y., Huang, Y. C., Liang, Y., Chen, C. C., Yu, J. S. and Chang, Y. S. (2011). Proteome-wide dysregulation by PRA1 depletion delineates a role of PRA1 in lipid transport and cell migration. *Mol. Cell Proteomics* **10**, M900641-MCP200.

Loftus, S. K., Morris, J. A., Carstea, E. D., Gu, J. Z., Cummings, C., Brown, A., Ellison, J., Ohno, K., Rosenfeld, M. A., Tagle, D. A. et al. (1997). Murine model of Niemann-Pick C disease: mutation in a cholesterol homeostasis gene. *Science* **277**, 232-235.

MacDonald, C., Buchkovich, N. J., Stringer, D. K., Emr, S. D. and Piper, R. C. (2012). Cargo ubiquitination is essential for multivesicular body intralumenal vesicle formation. *EMBO Rep.* **13**, 331-338.

Miaczynska, M., Pelkmans, L. and Zerial, M. (2004). Not just a sink: endosomes in control of signal transduction. *Curr. Opin. Cell Biol.* **16**, 400-406.

Mukhopadhyay, D. and Riezman, H. (2007). Proteasome-independent functions of ubiquitin in endocytosis and signaling. *Science* **315**, 201-205.

Nelissen, K., Mulder, M., Smets, I., Timmermans, S., Smeets, K., Ameloot, M. and Hendriks, J. J. (2012). Liver X receptors regulate cholesterol homeostasis in oligodendrocytes. *J. Neurosci. Res.* **90**, 60-71.

Okuda, T., Higashi, Y., Kokame, K., Tanaka, C., Kondoh, H. and Miyata, T. (2004). Ndrg1-deficient mice exhibit a progressive demyelinating disorder of peripheral nerves. *Mol. Cell. Biol.* **24**, 3949-3956.

Okuda, T., Kokame, K. and Miyata, T. (2008). Differential expression patterns of NDRG family proteins in the central nervous system. *J. Histochem. Cytochem.* **56**, 175-182.

Piper, R. C. and Katzmann, D. J. (2007). Biogenesis and function of multivesicular bodies. *Annu. Rev. Cell Dev. Biol.* **23**, 519-547.

Piquemal, D., Joulia, D., Balaguer, P., Basset, A., Marti, J. and Commes, T. (1999). Differential expression of the RTP/Drg1/Ndr1 gene product in proliferating and growth arrested cells. *Biochim. Biophys. Acta* **1450**, 364-373.

Raiborg, C. and Stenmark, H. (2009). The ESCRT machinery in endosomal sorting of ubiquitylated membrane proteins. *Nature* **458**, 445-452.

Reddy, J. V., Ganley, I. G. and Pfeffer, S. R. (2006). Clues to neuro-degeneration in Niemann-Pick type C disease from global gene expression profiling. *PLoS ONE* **1**, e19.

Roberts, R. C., Peden, A. A., Buss, F., Bright, N. A., Latouche, M., Reilly, M. M., Kendrick-Jones, J. and Luzio, J. P. (2010). Mistargeting of SH3TC2 away from the recycling endosome causes Charcot-Marie-Tooth disease type 4C. *Hum. Mol. Genet.* **19**, 1009-1018.

Saher, G., Brügger, B., Lappe-Siefke, C., Möbius, W., Tozawa, R., Wehr, M. C., Wieland, F., Ishibashi, S. and Nave, K. A. (2005). High cholesterol level is essential for myelin membrane growth. *Nat. Neurosci.* **8**, 468-475.

Scotti, E., Hong, C., Yoshinaga, Y., Tu, Y., Hu, Y., Zelcer, N., Boyadjian, R., de Jong, P. J., Young, S. G., Fong, L. G. et al. (2011). Targeted disruption of the idol gene alters cellular regulation of the low-density lipoprotein receptor by sterols and liver x receptor agonists. *Mol. Cell. Biol.* **31**, 1885-1893.

Sidiropoulos, P. N., Miehe, M., Bock, T., Tinelli, E., Oertli, C. I., Kuner, R., Meijer, D., Wollscheid, B., Niemann, A. and Suter, U. (2012). Dynamin 2 mutations in Charcot-Marie-Tooth neuropathy highlight the importance of clathrin-mediated endocytosis in myelination. *Brain* **135**, 1395-1411.

Sivars, U., Aivazian, D. and Pfeffer, S. R. (2003). Yip3 catalyses the dissociation of endosomal Rab-GDI complexes. *Nature* **425**, 856-859.

Sorrentino, V. and Zelcer, N. (2012). Post-transcriptional regulation of lipoprotein receptors by the E3-ubiquitin ligase inducible degrader of the low-density lipoprotein receptor. *Curr. Opin. Lipidol.* **23**, 213-219.

Staub, O. and Rotin, D. (2006). Role of ubiquitylation in cellular membrane transport. *Physiol. Rev.* **86**, 669-707.

Stendel, C., Roos, A., Kleine, H., Arnaud, E., Ozçelik, M., Sidiropoulos, P. N., Zenker, J., Schüpfer, F., Lehmann, U., Sobota, R. M. et al. (2010). SH3TC2, a protein mutant in Charcot-Marie-Tooth neuropathy, links peripheral nerve myelination to endosomal recycling. *Brain* **133**, 2462-2474.

Stuffers, S., Sem Wegner, C., Stenmark, H. and Brech, A. (2009). Multivesicular endosome biogenesis in the absence of ESCRTs. *Traffic* **10**, 925-937.

Sugii, S., Reid, P. C., Ohgami, N., Du, H. and Chang, T. Y. (2003). Distinct endosomal compartments in early trafficking of low density lipoprotein-derived cholesterol. *J. Biol. Chem.* **278**, 27180-27189.

Trajkovic, K., Hsu, C., Chiantia, S., Rajendran, L., Wenzel, D., Wieland, F., Schwille, P., Brügger, B. and Simons, M. (2008). Ceramide triggers budding of exosome vesicles into multivesicular endosomes. *Science* **319**, 1244-1247.

van Belzen, N., Dinjens, W. N., Diesveld, M. P., Groen, N. A., van der Made, A. C., Nozawa, Y., Vlietstra, R., Trapman, J. and Bosman, F. T. (1997). A novel gene which is up-regulated during colon epithelial cell differentiation and down-regulated in colorectal neoplasms. *Lab. Invest.* **77**, 85-92.

van der Goot, F. G. and Gruenberg, J. (2006). Intra-endosomal membrane traffic. *Trends Cell Biol.* **16**, 514-521.

Verhoeven, K., De Jonghe, P., Coen, K., Verpoorten, N., Auer-Grumbach, M., Kwon, J. M., FitzPatrick, D., Schmedding, E., De Vriendt, E., Jacobs, A. et al. (2003). Mutations in the small GTP-ase late endosomal protein RAB7 cause Charcot-Marie-Tooth type 2B neuropathy. *Am. J. Hum. Genet.* **72**, 722-727.

Wang, Y., Huang, Y., Hobbs, H. H. and Cohen, J. C. (2012). Molecular characterization of proprotein convertase subtilisin/kexin type 9-mediated degradation of the LDLR. *J. Lipid Res.* **53**, 1932-1943.

Wicher, G. and Aldskogius, H. (2008). Megalin deficiency induces critical changes in mouse spinal cord development. *Neuroreport* **19**, 559-563.

Zelcer, N., Hong, C., Boyadjian, R. and Tontonoz, P. (2009). LXR regulates cholesterol uptake through Idol-dependent ubiquitination of the LDL receptor. *Science* **325**, 100-104.

Zhang, L., Reue, K., Fong, L. G., Young, S. G. and Tontonoz, P. (2012). Feedback regulation of cholesterol uptake by the LXR-IDOL-LDLR axis. *Arterioscler. Thromb. Vasc. Biol.* **32**, 2541-2546.

Zhao, S., Hu, X., Park, J., Zhu, Y., Zhu, Q., Li, H., Luo, C., Han, R., Cooper, N. and Qiu, M. (2007). Selective expression of LDLR and VLDLR in myelinating oligodendrocytes. *Dev. Dyn.* **236**, 2708-2712.